18

Multiphysics Modelling and Simulation in Engineering

Alexandru M. Morega[1] and Juan C. Ordonez[2]
[1]*POLITEHNICA University of Bucharest,* [2]*Florida State University*
[1]*Romania,* [2]*USA*

1. Introduction

As more and more complex and sophisticated hardware and software tools are available, complex problems described by consistent mathematical models are successfully approached by numerical simulation: modelling and simulation are present at almost each level in education, research, and production. Numerical "experiments" have predictive value, and complement physical experiments. They are unique in providing valuable insights in *Gedankenexperiment*-class (thought experiment) investigations.

This chapter presents numerical simulation results related to a structural optimization problem that arises in systems with gradients and fluxes. Although the discussion concerns the optimal electrical design of photovoltaic systems, it may be extended to a larger class of applications in electrical and mechanical engineering: diffusion and conduction problems.

The first concern in simulation is the proper formulation of the physical model of the system under investigation that should lead to consistent mathematical models, or *well-posed* problems (in Hadamard sense) (Morega, 1998). When available, analytic solutions – even for simplified mathematical models – may outline useful insights into the physics of the processes, and may also help deciding the numerical approach to the solution to more realistic models for the systems under investigation. Homemade and third party simulation tools are equally useful as long as they are available and provide for accurate solutions.

Recent technological progresses brought into attention the *Spherical PhotoVoltaic Cells* (SPVC), known for their capability of capturing light three-dimensionally not only from direct sunlight but also as diffuse light scattered by the clouds or reflected by the buildings. This chapter reports the structural optimization of several types of spherical photovoltaic cells (SPVC) by applying the constructal principle to the minimization of their electrical series resistance. A numerically assisted step-by-step construction of optimal, minimum series resistance SPVC ensembles, from the smallest cell (called *elemental*) to the largest assembly that relies on the minimization of the maximum voltage drop subject to volume (material) constraints is presented. In this completely deterministic approach the SPVC ensembles shapes and structures are the outcome of the optimization of a volume to point access problem imposed as a design request.

Specific to the constructal theory, the optimal shape (geometry) and structure of both natural and engineered systems are morphed out of their functionality and resources, and of the constraints to which they are subject.

2. Shape and structure out of a multiphysics principle

The development of the *constructal principle* (Bejan, 2000) relies on the analysis of natural dynamic systems with fluxes and gradients (*e.g.*, temperature, pressure, electric potential, chemical potential, etc.) that, internally, are outside thermodynamic equilibrium. A second important aspect is that the variety of geometrical natural forms, which we may recognize and which are found in both animate and inanimate worlds, is not that vast: *natural systems may have the same geometric shape without being identical*. For instance, two bronchial trees are never identical. Basically, when these systems are presented by a single image out of the endless diversity of natural flow forms we have the ability to recognize and classify them as *tree*, *round* and *slice*. If one single principle explains all these forms then it may act everywhere, and it becomes a law that ties different areas such as physics and biology or, better said, two different modes of reasoning, two different points of view.
The constructal principle is used in this work to produce architectures (shapes, structures) based on the optimization of the systems under investigation – purpose, function – rather than by conjectural assumptions.

2.1 Functional objective and constraints

Spatial and temporal structures observed in Nature are the results of global optimization subject to local and global constraints: a finite-size heterogeneous system undergoes changes in shape and structure such as to provide for an as easy as possible access, or low impedance paths, of its internal fluxes. Optimization principles such as minimum travel time, minimum flow resistance, minimum power consumption are invoked and used, and it is remarkable that these deterministic principles are independent, and do not follow up, do not result, from other, known laws.
Engineering design starts by a clear understanding of the *objective*: the system mission, its purpose, function and performance. The design's objective implies also *optimization*, because the engineered system is expected to perform the best *possible*. Possible means that there are *local* and *global* constraints (limitations) that the system may have.
Examples of some very common *global* constraints are the system mass and volume; the heat generated within the occupied volume, *e.g.*, by an electronic ensemble, is another global constraint when the electronic components have to fit within an imposed volume.
The *local* constraints are more subtle, but equally important. For instance, in a system with internal heat generation (*e.g.*, a cable that carries electric current, electronic devices, etc.) the maximum temperature is not to exceed a certain safe limit. From this perspective, the number and localization of the hot spots is not important. The local constraints may then be gathered in an *objective function* defined at the system level. The geometry is the unknown. The external shape and the internal structure emerge then by recurrent, iterative design.
In the constructal theory, the deterministic evolution occurs in time, from principle (engineering) to Nature. The history of science and technology abounds in examples where the sense is the opposite *i.e.*, from Nature to engineering – this method is recognized today as *Biomimetics*, and it continues to be a valuable instrument in engineering design. Compared to Biomimetics, constructal theory acts in the opposite sense: the engineering generates a purely theoretic point of view, from which Nature may be better understood, *i.e.* more simply. And this is consistent with Poinacré's conclusion: "C'est là la simplicité cachée, celle qu'il faut découvrir" (Poincare, 1902).

2.2 Fermat's principle; constructal principle

Fermat's principle, used only in optics (Lemmons, 1997), postulates that light, which propagates between two points (A,B) located in different optical media, must choose the path that minimizes the travel time. It follows then that the angle of refraction, $\sin\beta_i / \sin\beta_r = \nu_{i,r}$, is an optimization result, where $\nu_{i,r}$ is the refraction index relative to the two media. Fermat's principle covers the much older principle of the shortest path postulated by Heron of Alexandria: *light propagates following a straight path and the incident angle at a mirroring interface is equal to the reflection angle*.

By contrast to the point-to-point "flow" law of Fermat and Heron, the constructal law refers to finite size systems with internal flow generation, from the volume (an infinite number of points) to a sink (M) located on the boundary.

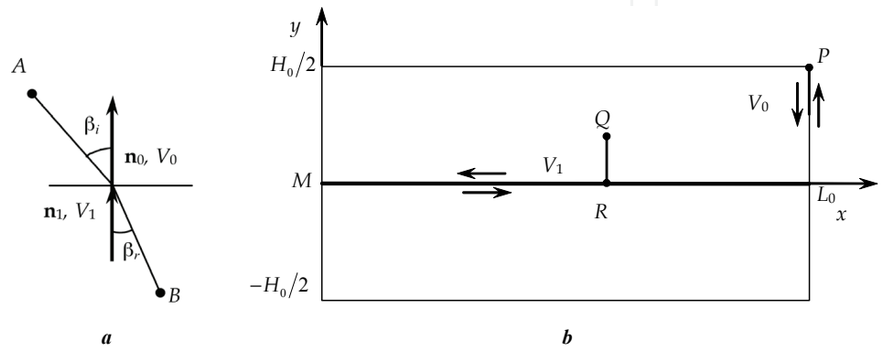

Figure1. Fermat's (a), and constructal (b) optimal access principles

In Figure 1 the volume is represented by a rectangle of area $A_0 = H_0L_0$, called *elemental system*. The size of A_0 is fixed, but the aspect ratio H_0/L_0 may vary. The system is made of two media, where motion may occur at two speeds, $V_0 << V_1$. The amount of high-speed material (V_1) is small and fixed – much smaller than the rest of volume occupied by the low-speed material, (V_0), with internal generation (*e.g.*, heat, current, etc.).

The objective of the elemental cell finite-size system optimization consists of maximizing the volume-to-point access between all points of A_0 and M. The geometric shape and the internal structure of A_0 (*i.e.*, the distribution of high speed material throughout the low-speed material) are then natural results. The global constraints are the fixed size of the system and the amount of high permeability material to be distributed within the system. On the other hand, some of the internal points will always have easier access to M than other points. The longest trip to M is associated to the most distant point in A_0 (point P in Fig. 1), which is then the most solicitated point – it is the analogous to the point of highest mechanical stress in a mechanical structure or the hottest spot in a thermal structure. The design may be improved by changing the external aspect ratio, to produce more uniform access to the volume from M.

The constructal optimization works similarly to Fermat's principle that anticipates the geometric shape of the light beam. Unlike Fermat's principle where the trajectory is broken at the interface between the two semi-infinite media, in the volume-to-point access problem the bent (*e.g.*, R) is found on the central axis of A_0, and this is the result of an optimization principle. The volume-to-point construct is then a bundle of an infinite number of flow paths that verifies Fermat's principle.

At this point we may introduce the fundamental constructal problem: *"Given a finite size*

volume with internal heat generation and of low conductivity, which is cooled by a small-size sink placed on the boundary, distribute a fixed amount of high conductivity material within the volume such that the hotspot temperature is minimum" (Bejan, 2000). In other words, find the shape and structure that minimize the system's thermal resistance.

For instance, electronic structures (packages) are subject to thermal objectives and constraints. The global constraint is the finite volume where the system must fit. The thermal design objective consists of installing as many components as possible, hence an as high as possible heat generation rate, q (electrical structures generate heat). The maximum temperature in the systems may not exceed a specified limit, T_{max} – this is the local constraint. The optimal design is then superior if q is large, *i.e.* the global thermal conductance $q/(T_{max}–T_0)$ is high – T_0 is the initial temperature of the environment that absorbs the heat.

3. Photovoltaic cells optimization – a design problem

The interest on PhotoVoltaic Cells (PVC) has increased recently due to the energy crisis and the advance of the alternative energies. Solar cell power generation systems installed in 2000 has reached 711 MW worldwide, and in the future it is expected to grow (Kyosemi, 2006). As over 90% of the nowadays PVCs use polysilicon as a raw material, the recent shortages of high-grade silicon will significantly impact on the growth of the PV industry.

PVCs are semiconductor devices, made of two sandwiched layers of intrinsic semiconductors of p and n–type that convert light directly into electricity. The photons absorbed by the PVC wafer generate electric charges (electrons and holes) that are drained across the p-n junction in opposite directions by the action of an electric field produced by the photovoltaic effect. This segregation generates a voltage across the junction that may conduct a current in an external load (CPE-UNSW, 2004), (EMSOLAR, 2004).

Partial reflection of the incident light, the incomplete absorption and utilization of the photons energy, the partial recombination of electrical charge carriers and the leakage across the junction (Burgers & Eikelboom, 1997), (Green, 1986), (Horzel & De Clerq, 1995), (Verbeek & Metz, 1996), (STARFIRE, 2002) are main factors that reduce the PVC efficiency. The power loss occurs in the bulk of the base material, R_p (Fig. 2a), in the narrow top-surface layer, at the interface between the cell and the electrical terminals of the PVC.

The cell series resistance, R_S (Fig. 2a), met by the lateral current in the cell's top layer is responsible for the flattening of the current-voltage characteristic (Fig. 2b) and for the corresponding PVC output power loss. It may be reduced by using a highly conductive material for the top layer (or window), by increasing its thickness, by good galvanic contacts and by optimized geometry for the contact electrode grid (STARFIRE, 2004), (EMSOLAR, 2004).

The front collector – a finger-like metallic contact connected to a busbar system – is to reduce R_S. Unfortunately, this structure prevents the incident radiation to reach the cell: large electrical contacts may minimize R_S, but they would cover the cell and block too much of the light. An optimal design is then a compromise between an as low as possible R_S (closely spaced, highly conductive grid with good adhesion and low R_S) and an as high as possible light transmission (fine, widely spaced fingers). Currently, the acceptable loss from the contact shading is 10% in commercial cells (EMSOLAR, 2004), (STARFIRE, 2002, 2004).

The series resistance optimisation consists of minimising the *sum* of the collector shadow and resistance (Joule) losses and, despite the many physical processes within the PVC

(Altermatt et al., 1977) it may be conducted separately (Radike et al., 2002). Instead of the double diode description of the PVC, we used the *maximum power point* (MPP) (Fig. 2,c) approach (Burgers & Eikelboom, 1997), which allows for the PVC to be optimised for either a specific or a mix of irradiation levels, such as it occurs under normal working conditions.
In addition, the optimal design of the collector has to comply with criteria such the aesthetic appearance, and several collector patterns derived from the flat-surface *H*-type PVC were proposed (Radike et al., 2002).

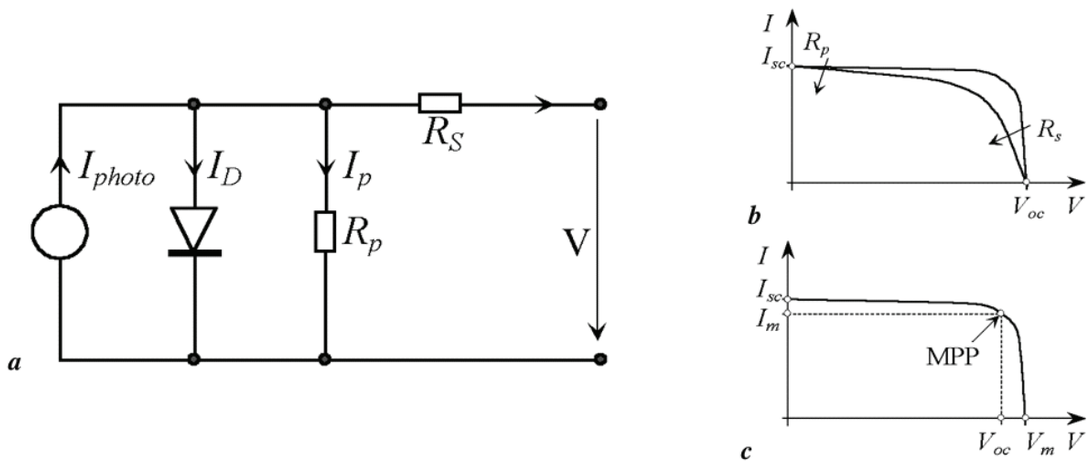

Figure 2. An equivalent circuit for a hetero-junction PVC: (a) Equivalent scheme; (b) The effect of R_p and R_S; (c) Maximum power point, MPP [13]

As seen in the previous subsection, constructal theory is based on the thought that architecture comes from a principle of maximization of flow access for both animate and inanimate flow systems. The theory provides a framework to design and analyze finite-size, constraint systems. We apply this strategy to connect an area with PV current generation to a terminal, with the objective of draining the generated current throughout a minimum resistance path.
The basic volume-to-point access problem has an equivalent electrokinetic formulation (Morega & Bejan, 2005), (Morega et al., 2006a, 2006b): *given a finite size volume in which electrical current is generated at every point, which is connected by a small patch (terminal) located on its boundary, and a finite amount of high (electrical) conductivity material, find the optimal distribution of high conductivity material in a given volume so that the peak voltage is minimized.*

3.1 The mathematical model in the PVC series resistance optimization

We assume that the PVC operates under DC conditions hence the associated electric field is potential. For the *n*-layer of the PVC the current flow in the emitter and metallic collector is essentially 2D. By Ohm's law, the total current density is

$$\mathbf{J} = \sigma_{0,p}\left(\mathbf{E}+\mathbf{E}_i\right) = -\sigma_{0,p}\nabla V + \sigma_{0,p}\mathbf{E}_i = -\sigma_{0,p}\nabla V + \mathbf{J}_i \,. \tag{1}$$

Here, $\mathbf{J}_i$ is the photovoltaic current density (assumed uniform), $\sigma_{0,p}$ are the electrical conductivities of the collector and emitter, respectively (assumed linear, homogeneous and isotropic). The partial differential equations that give the electrical field are obtained by setting to zero the divergence of the total current density

$$\frac{\partial^2 V}{\partial X^2}+\frac{\partial^2 V}{\partial Y^2}+\frac{1}{\sigma_0}w'''=0, \text{ emitter} \tag{2}$$

$$\frac{\partial^2 V}{\partial X^2}+\frac{\partial^2 V}{\partial Y^2}=0, \text{ collector} \tag{3}$$

Here, $w'''=\text{div}\,\mathbf{J}_i$, and $\mathbf{J}_i$ are known quantities.. Except for the output port through which the current exits the cell (set at ground potential, a Dirichlet condition), the boundary is assumed electrically insulated (a Neumann homogeneous condition).
This electrokinetic problem is equivalent to the conduction heat transfer problem, with the correspondence $T\leftrightarrow V$, $q'''\leftrightarrow w'''$, $k_0\leftrightarrow\sigma_0$, $k_p\leftrightarrow\sigma_p$ (k_p, k_0 are the thermal conductivities of the collector and emitter, respectively). The electrically insulated boundary is equivalent to adiabatic boundaries (Bejan, 1997b), (Ordonez et al., 2003).
Next, we present the constructal growth for the flat surface PVC, from the elemental cell to higher order ensembles. Numerical simulations are validated against analytic solutions, and then used in more realistic circumstances.

3.2 Flat-surface PVC optimization – an analytic solution

(a) The elemental system

Figure 3 shows the PV smallest system, called elemental system. We consider a rectangular PV cell and its metallic collector (finger), situated on the long symmetry axis. Except for the port at the origin, the boundary is electrically insulated.

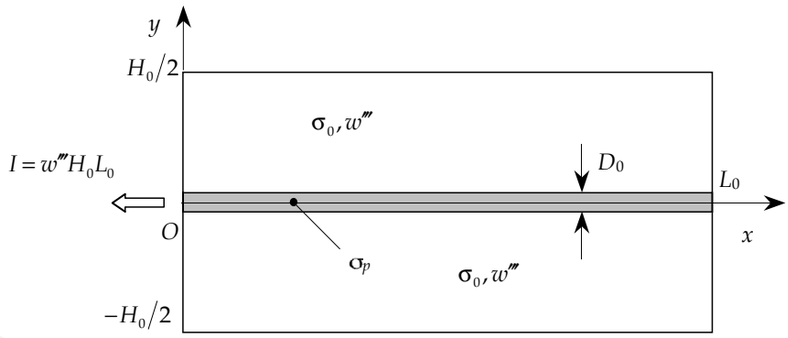

Figure 3. The elemental system with internal PV current generation, and its metallic collector

The cell area $A_0=H_0L_0$ and the area of the metallic grid, A_p, are kept constant throughout the optimization. However, H_0 and L_0 may vary and, as H_0 << L_0, it follows that the current in the emitter flows mainly in y direction, to be then collected by the σ_p finger at $y=0$ and drained in x direction – this assumption is discarded in the numerical model.
The closed form solution to the problem of the current flow in the PVC emitter – eq. (4), $\partial V/\partial y\big|_{y=H_0/2}=0$, $V(x,0)=V_0(x)$ – is $V(x,y)=\dfrac{w'''}{2\sigma_0\left(H_0y-y^2\right)}+V_0(x,y)$. The closed form solution to the problem of the current flow in the PVC collector – $\sigma_P D_0 d^2V/dx^2+w'''H_0=0$,

$V_0\big|_{x=0} = V(0,0)$, $\left.\frac{dV_0}{dx}\right|_{x=L_0} = 0$ – is $V(x,y) - V(0,0) = \frac{w'''}{2\sigma_0}\left(H_0 y - y^2\right) + \frac{w''' H_0}{\sigma_P D_0}\left(L_0 x - \frac{x^2}{2}\right)$ (Morega & Bejan, 2005).

Using these results, it may be inferred that the maximum voltage drop on the elemental cell, ΔV_0, has a minimum with respect to the cell shape (H_0/L_0)

$$\frac{\Delta V_{0,min}}{w''' H_0 L_0/\sigma_0} = \frac{1}{2}\left(\frac{\sigma_0 H_0}{\sigma_P D_0}\right)^{1/2}, \quad \left(\frac{H_0}{L_0}\right)_{opt} = 2\left(\frac{\sigma_0 H_0}{\sigma_P D_0}\right)^{1/2}. \tag{4}$$

This conclusion is consistent with the assumption that the elemental system is slender, suggesting that $\sigma_P/\sigma_0 >> H_0/D_0 >> 1$.

Two additional properties of this *geometric* optimization are remarkable (Bejan, 1997b):

1. *The principle of equipartition*: the voltage drop in the emitter equals the voltage drop along the finger, *i.e.*, $\Delta V_{0,min}$ is divided in half by the bend ($x = L_0$, $y = 0$).
2. At the elemental level, the voltage drop, $\Delta V_{0,min} = w''' H_0^2/(4\sigma_0)$, decreases as H_0^2. This motivates the effort to manufacture the smallest possible elemental system.

(b) The first order ensemble

Figure 4 shows the first order ensemble, where the D_0 fingers are connected to the D_1 current path, called *busbar*. The boundary is insulated, except for the terminal of size D_1 at the origin, where the collected current leaves the structure. The new optimization problem is to find how many elemental volumes to assemble, or the optimal shape $H_1 \times L_1$, such that the maximum value of the voltage drop in the assembly from a point to the origin is minimal.

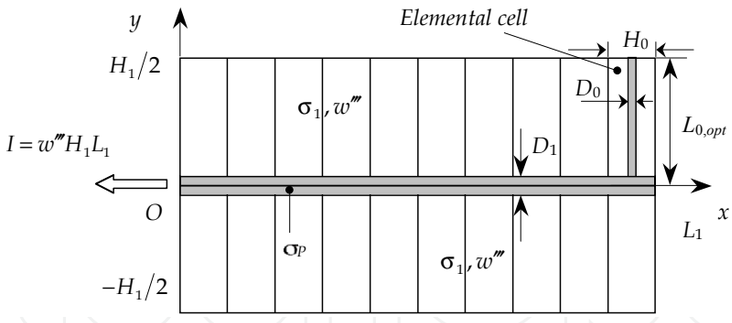

Figure 4. The first construct made of optimized elemental systems

In a volume-average sense, the ensemble behaves as the σ_0 region, except that its effective conductivity is $\sigma_1 = \sigma_P D_0/H_0$.

A similar analysis may be conducted to calculate the voltage drop on the first order ensemble, ΔV_1. Its maximum has a minimum, $\Delta V_{1,min} = w''' H_0^2/4\sigma_0$, registered between the farthest corner $(L_1, H_1/2)$ and the exit port at the origin, (0,0).

The resistance of the ensemble is then minimized by using the principle of equipartition, with the constraint $\phi_1 = A_{p,1}/(H_1 L_{1,opt})$, where $A_{P,1} = D_1 L_{1,opt} + n_{1,opt} D_0 L_{0,opt}$ is the area of

high conductivity material (ϕ_1 is sometmes called *porosity*) (Morega & Bejan, 2005), yielding $\Delta V_{a_1,min} = (3/8)\left(w'' H_0^2/\sigma_0\right)$. Apparently, the busbar has to be wider than the fingers, and $(D_1/D_0)_{opt} = \left[(D_0\sigma_P)/H_0\sigma_0\right]^{1/2} >> 1$.

An important result of this analysis is the *scalability* of the construct: the voltage drop on the optimized ensemble is *almost equal* to the optimized voltage drop on the elemental system.

A *twice* optimized, first order ensemble – with respect to the $H_1 \times L_1$ shape *and* to the allocation of high conductivity material – is then obtained for the optimal number of fingers $n_{1,opt} = \left[(\sigma_P/\sigma_0)(D_0/H_0)\right]^{1/2} >> 1$ and for the busbar length $L_{1,opt} = (1/2)\left(H_0 D_0 \sigma_p/\sigma_0\right)^{1/2}$.

Remarkably, the optimal shape of this ensemble is a constant, $(H_1/L_1)_{opt} = 2$, independent of the type of conducting materials (σ_P/σ_0) and of the proportion in which (ϕ_1) they are built into the ensemble. Consequently, *the optimal shape* $H_1 \times L_1$ *is such that a square of side* L_1 *forms on either side of the* D_1 *busbar* (x axis). By using $H_1 = 2L_{0,opt}$, it yields $(L_1/L_0)_{opt} = 1$.

(c) Second and higher order ensembles

The best *second order ensemble* (Fig. 5a) is made of two optimized first order ensembles patched such that $H_2 = H_1 = 2L_{1,opt} = 2L_2$. The D_1 wide strip is the D_1 wide busbar in Fig. 4.

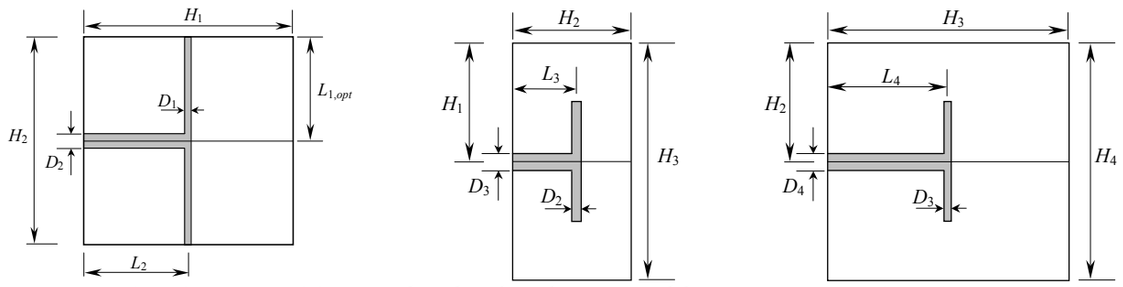

a. Second order ensemble b. Third order ensemble c. Fourth order ensemble

Figure 5. Second to fourth order ensembles: made of two optimized lower order constructs

The best *third order assembly* (Fig. 5b) may be obtained by a double optimisation (geometric shape *and* busbar width) of a system made of optimised second order ensembles. Figure 5c shows the fourth order ensemble made of two third order ensembles

Apparently, in the process of optimization the finger width doubles from one ensemble to the next, higher order one, outlining the following relations, where i is the ensemble order (Morega & Bejan, 2005)

$$D_{i,opt} = \frac{2^i}{3^{1/2}} D_0 \left(\frac{D_0\sigma_p}{H_0\sigma_0}\right)^{1/2} \quad \text{for } i \geq 2, \tag{5}$$

$$L_i = 2^{\frac{i}{2}-m}\left(H_0 D_0 \frac{\sigma_p}{\sigma_0}\right)^{1/2}, \; i \geq 3, \; m = \begin{cases} 2, & i \text{ even} \\ 5/2, & i \text{ odd} \end{cases} \tag{6}$$

$$H_i = 2^{\frac{i}{2}-p} H_0 \left(\frac{D_0 \sigma_p}{H_0 \sigma_0} \right)^{1/2}, \; i \geq 2, \; p = \begin{cases} 1, & i \text{ even} \\ 1/2, & i \text{ odd} \end{cases} \tag{7}$$

$$\phi_i = \phi_{i-1} + \frac{2^{(i-2r)/2}}{3^{1/2}} \frac{D_0}{H_0}, \quad i \geq 3, \quad r = \begin{cases} 0, & i \text{ even} \\ 1/2, & i \text{ odd} \end{cases} \tag{8}$$

$$\Delta V_{a_i,min} = \frac{3}{16} \frac{\phi_i}{D_0/H_0} \frac{w''' H_0^2}{\sigma_0}. \tag{9}$$

Figure 6a shows the optimised fourth order ensemble with its constituent parts, including the elemental cells (the strips). The number of such striations is *not* a constant, and it depends on $2\left(\sigma_0 H_0 / \sigma_P D_0\right)^{1/2}$. Another important feature is that the width of the optimised busbar increases with the ensemble order. Figure 7 shows the high order end of the optimised construction sequence.

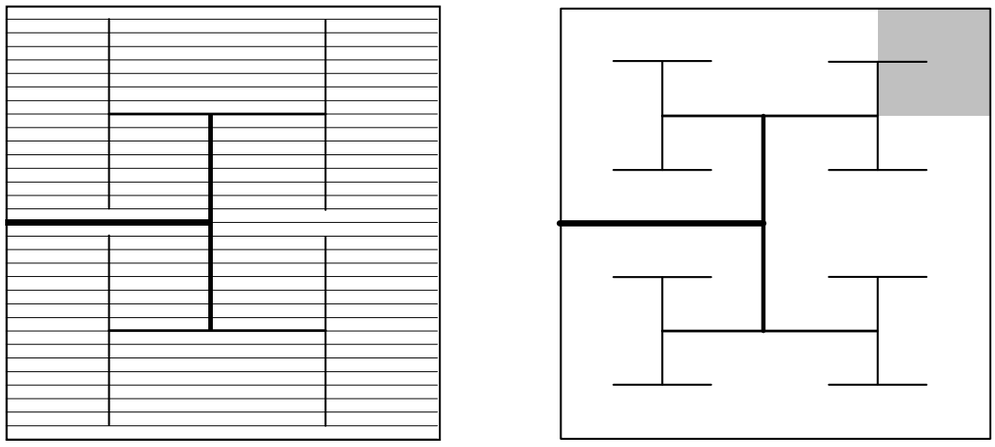

a. Fourth order ensemble

b. Eighth order ensemble – the fourth order ensemble is marked in grey

Figure 7. Optimized networks of higher-order ensembles – designs based on analytic solutions

3.3 H-type PVC optimization – numerical simulation solution

The analytical work may be accompanied by numerical simulation. First, eqs. (2), (3) are non-dimensionalized

$$\Delta v + 1 = 0, \text{ emitter} \tag{10}$$

$$\Delta v = 0, \text{ collector} \tag{11}$$

by dividing the coordinates with the length scale, $\sqrt{H_0 L_0}$, the current source with $w''' = \operatorname{div} \mathbf{J}_i$, and the electrical conductivities of the emitter and collector with σ_0. It follows

then that the voltage scale is $V_0 = w''' H_0 L_0 / \sigma_0$. In the optimization process of the 2D flat-surface PV ensembles the laplacian [eqs. (10), (11)] is defined as $\Delta v = \partial^2 v / \partial x^2 + \partial^2 v / \partial y^2$.

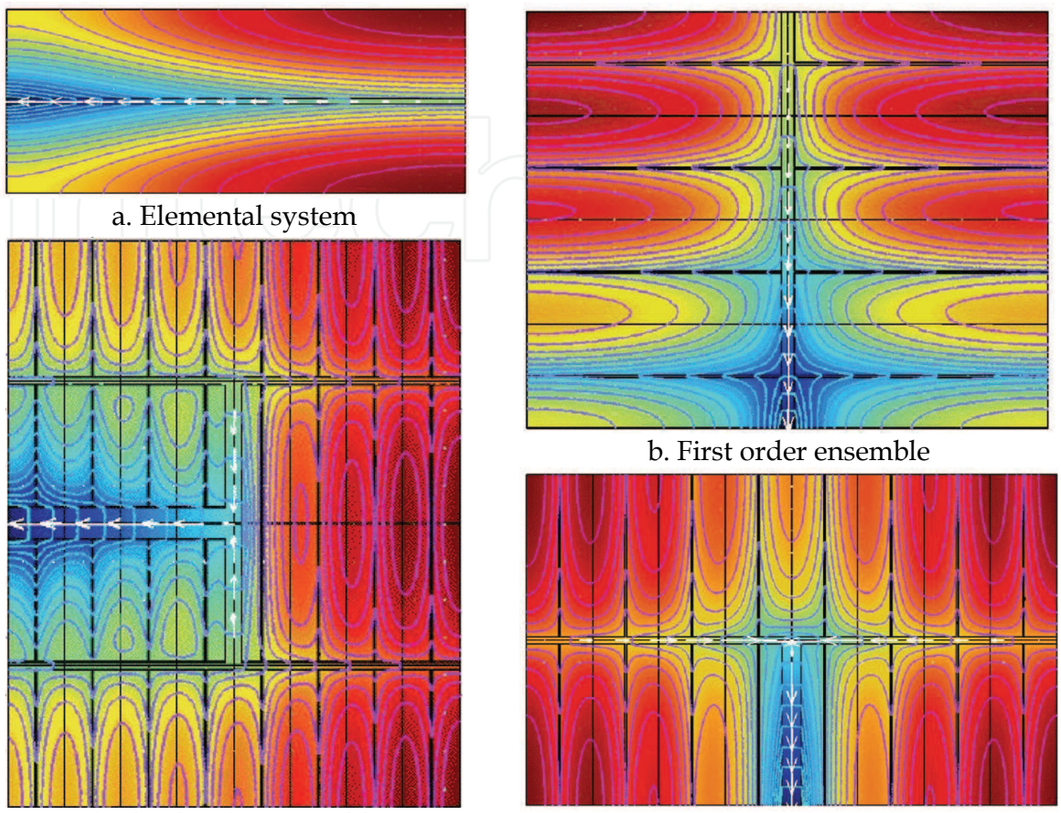

a. Elemental system

b. First order ensemble

d. Third order ensemble

c. Second order ensemble

Figure 8. Optimized networks of higher-order ensembles – numerical simulations

To check the first five steps of the procedure we used a finite element software (Comsol, 2004-2008) that implements Galerkin-Lagrange technique. The meshes we used were unstructured, Delaunay-type. Figure 8 displays the typical steps that follow the constructal optimization sequence, conducted for an elemental cell with $d_0 = 0.005, h_0 = 0.1, l_0 = 0.5$, and $\sigma_p / \sigma_0 = 1000$.

4. Spherical photovoltaic ensembles – structural optimization

A variety of *flat surface* PVCs, materials and manufacturing methods have been developed (CPS-UNSW, 2006). However, the incident sunlight to a solar cell varies according to the position of the sun, weather conditions, the objects around that reflect sunlight, and flat light reception surface cells (Fig. 9,a) cannot sufficiently meet these diverse conditions. Recently, novel Spherical PhotoVoltaic Cell (SPVC) technologies were developed (Fig. 9b,c) that capture sunlight three-dimensionally, not only as direct sunlight but also as light diffused by clouds, and as light reflected from buildings (Kyosemi, 2006), (Fujipream & Clean Venture, 2006), (SSP, 2006).

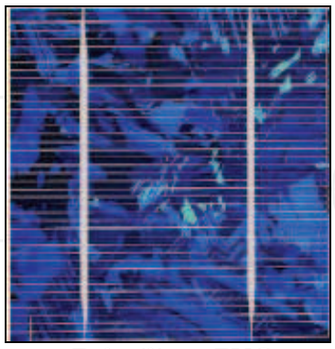

a. Polysilicon PVC – standard flat-surface "H" design

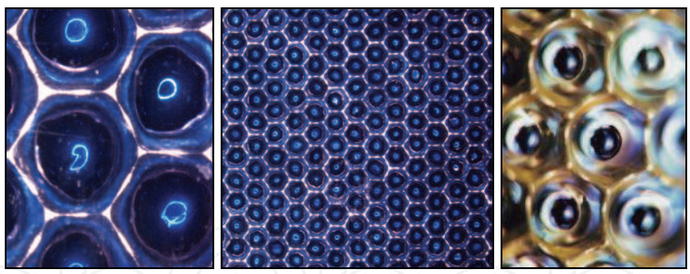

b. Spherical PVC – honeycomb Spherical by Solar Power array (Morega, 2006,1) and by Fujipream (Fujipream & Clean Venture, 2006)

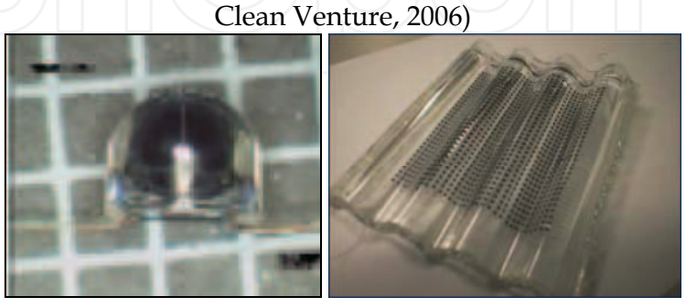

c. Spherical PVC – Kyoto Semiconductor Corporation (Kyosemi, 2006)

Figure 9. Flat-surface and SPVC ensembes

In contrast to flat-surface cells, Spherical Sunlight Reception Surfaces (SSRS) can receive light in all directions thus increasing their power generation capacity. They minimize the output fluctuations even under direct sunlight, and even when the angle of the reflected incident light changes. Practically non-directive, SSRS can increase their output power by improving the efficiency of light utilization, as there are fewer restrictions on their mounting. The SPVC consists of a single spherical *p-n* junction (Fig. 10).

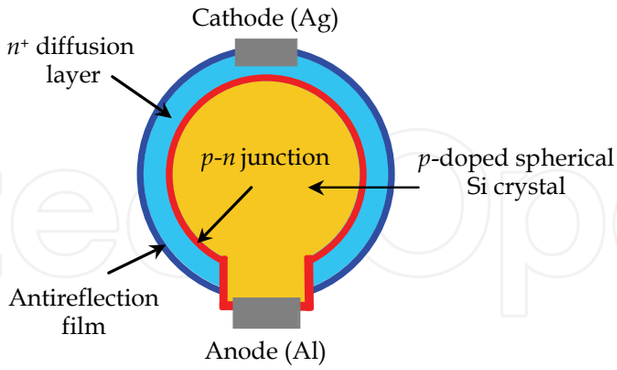

Figure 10. A spherical solar cell captures light in all directions – after (Kyosemi, 2006)

This technology uses less costly silicon, and gives more flexibility and ease of integration in different applications. The process starts with low cost silicon, which is the raw material used in the sphere fabrication process. The silicon is first purified and then formed into tiny spherical beads of proper size (Kyosemi, 2006). The diameter of a SPVC should be small in order to increase the proportion of the light reception surface area of the semiconductor crystal to its volume so as to raise the efficiency of the material (Morega et al., 2006a, 2006b).

Notably, the cells are spherical and thus excellent in mechanical strength. The mounting may be white resin reflection plate, with its surface covered with transparent resin.
Although very small (0.2–2mm), the SPVC maximum open voltage is the same as that of a larger flat junction type cell. SPV modules are produced in a variety of power needs ranging from an extremely small to a large power source – *e.g.*, through connection of cells in series and parallel with fine copper wire (Kyosemi, 2006).

4.1 Structural optimization of SPV ensembles by numerical simulation

The previous section reported the flat-surface PVC ensembles optimization. Unlike that case, here the design goal is to find either the particular pattern of the SPVCs distribution on a high conductivity material foil or a wireframe network that would connect the PV beads such that R_S is minimized. In both cases we consider the DC regime of the electric field.
The mathematical model (10), (11) with appropriate boundary conditions was solved numerically, by FEM technique (Comsol, 2004-2008), for the two different types of SPV modules: the *honeycomb* and the *interconnected* (*wired*) ensembles. First, the non-dimensional electrical field (v) is solved for. We used solvers that utilize the symmetry of the algebraic system generated by this linear problem. Then, two quantities are sought: the maximum voltage drop on the cell/ensemble (the maximum potential, v_{max}) and the series resistance, R_S, defined here as the ratio of v_{max} through the total current produced by the cell/ensemble. *The time-arrow of the design goes from the elemental system to higher order ensembles, following the constructal technique*

4.2 Honeycomb arrayed SPVC ensembles – a first model

The honeycomb (SSP, 2006) ensembles fabrication process involves bonding the tiny silicon spheres between sheets of thin and flexible substrates (usually aluminium) – Fig. 9*b*. The front foil acts as the cathode and determines the spacing of the spheres (Fig. 11), while the back foil acts as the anode to the core of the spheres (Morega et al., 2006a).

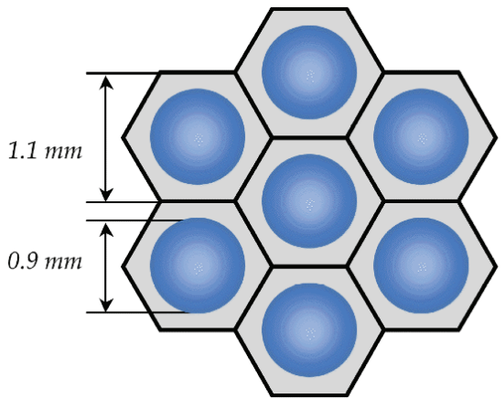

Figure 11. Honeycomb SPVC array

The optimization problem of the honeycomb packaging differs from the fundamental flat-surface PV problem in the sense that the (current) sources are spread throughout a very good conducting material, which embeds the PV beads and cannot be distributed in a spanning tree structure. Further more, the ensemble edges act as paths of high conductive material, draining part of the current generated by the SPV cells closer to the boundary.

Another difficulty related to this design – if modelled at the SPVC level – is the staggered arrangement itself. It appears more convenient – and within satisfactorily accuracy limits – to rely on average, equivalent 2D SPVC models. The first concern is then to define an equivalent elemental cell that consistently represents the actual SPVC (Fig. 5).

(a) Simplified 2D models for the spherical solar cell

First, a simplified 2D axial-symmetric model may be used to evaluate the current distribution through the *n*-layer of the SPV bead – Fig. 12b. The following boundary conditions may be used to close the Laplace problem for the electrical potential:

- On the inner surface of the shell (the *p*-*n* interface) a non-homogeneous Neumann condition defines the photovoltaic current source.
- The outer surface of the bead is electrically insulated.
- The contact between the bead and the aluminum foil collector is set at $V = 0$, because the excellent electrical conductivity of aluminum suggests an almost equipotential contact.

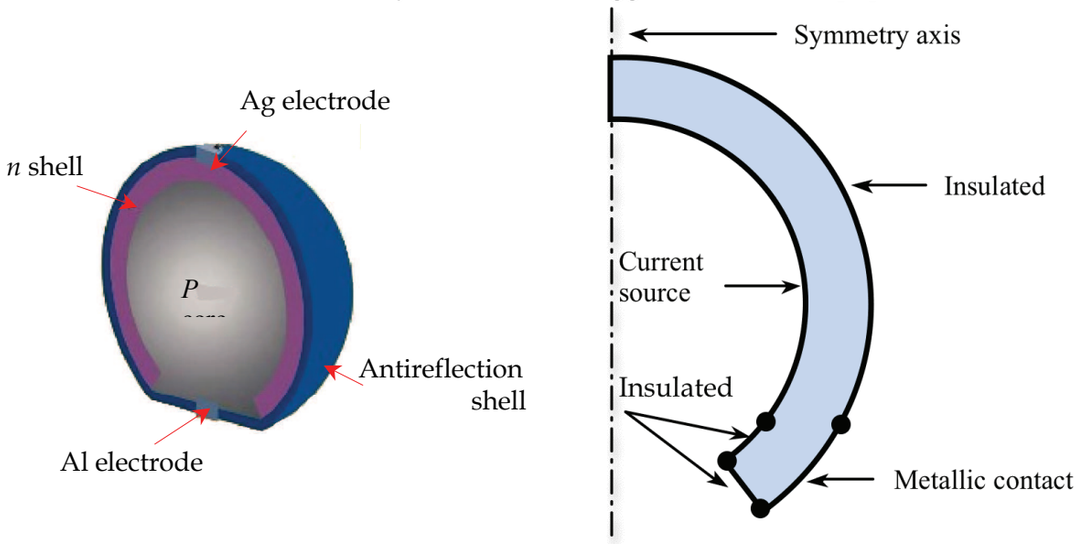

a. The spherical SPVC – after (Kyosemi, 2006) b. A simplified 2D axial-symmetric model

Figure 12. The SPCV bead – an equivalent 2D axial model and the BCs in the DC problem

This 2D axial model gives an estimate of the series resistance of the *n*-layer, which is part of the global series resistance of the SPVC.

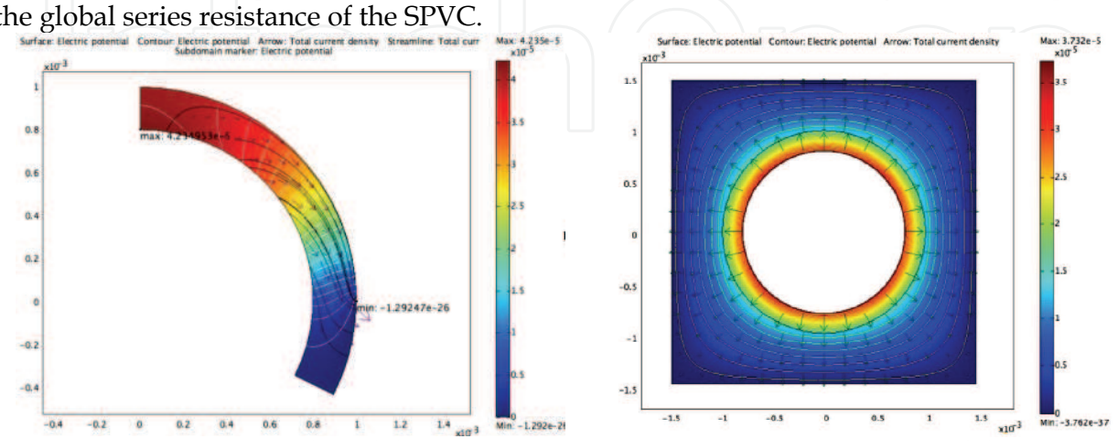

a. 2D Axial model b. 2D Cartesian model

Figure 13. The 2D equivalent models of a spherical solar cell – electric field spectra

Figure 13a shows the electrical field (voltage surface color map and equipotential contour lines), and the electric current flow (arrows and streamlines) within the shell, obtained by numerical simulation.

The next step is to "flatten" the 2D axial model, *i.e.* to recast it into a 2D Cartesian model that comprises also the collector (aluminum) "territory" of the bead: the *n* shell is projected onto a circular crown that has the same series resistance as the actual spherical layer; the inner rim of the crown produces the same amount of current as the inner boundary of the spherical *n*-shell. The actual size of the aluminum patch that embeds the bead may make the object of another optimization problem. Figure 13*b* depicts the voltage (surface color map and contour lines) and the current flow (arrows and streamlines) when the external boundary is set to ground. Of course, symmetry may be used to simplify the problem, but the numerical effort to solve this linear problem for the entire domain is not significant.

The 2D Cartesian model is further used to define the elemental cell of the structural optimization sequence. The elemental cell may contain a number of SP beads, and it is the smallest entity, the construct or "brick" that is optimized for minimum series resistance: *its shape and structure are essential to the shape and structure of higher order constructs in the optimization sequence*.

(b) The elemental system

The first elemental cell design we propose (Fig. 14a) is a simple system that, by constructal growth, may evolve into a staggered honeycomb SPVC ensemble (Fig. 11). It is assumed that the photovoltaic current leaves the cell through the vertices, and that the edges are electrically insulated. The only degree of freedom here is the relative position of the beads along the principal axes of the triangular surface, between vertices and the mass center.

The ratio between the peak-voltage, wherever it occurs, and the total current produced by the SPV beads, defines the series resistance of the cell, R_s. Its inverse, the series conductance, is a quality factor (*QF*), a design quantity. As R_s depends on the relative position of the beads, we carried out numerical experiments to find the layout that leads to its minimum.

Figure 14b shows the mesh produced by the adaptive algorithm used to solve the conduction problem. The circular interior boundaries are current source, and the vertices are patched with tiny metallic electrodes: they are the current ports to the structure.

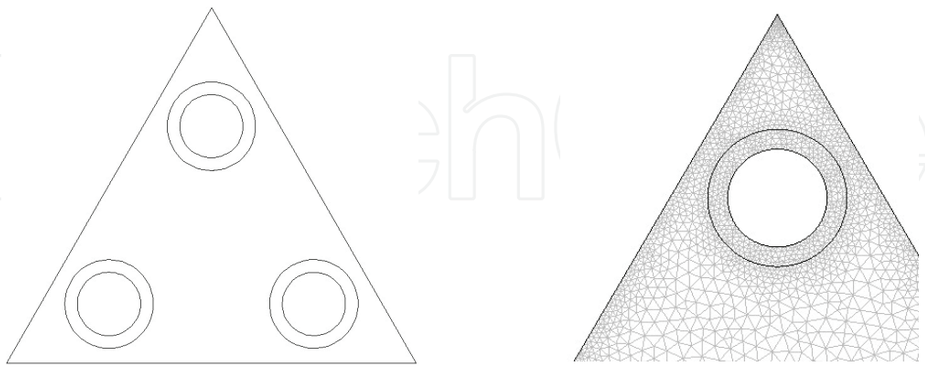

a. The elemental system b. The FEM mesh for elemental system – detail

Figure 14. The computational domain in the honeycomb SPV ensemble optimization

By symmetry grounds, the *optimal* elemental system should have the same type of symmetry. Figure 15 shows the voltage (surface map and contour lines), the current density (arrows), for three layouts, including the optimal design with highest *QF* (minimum, maximum voltage).

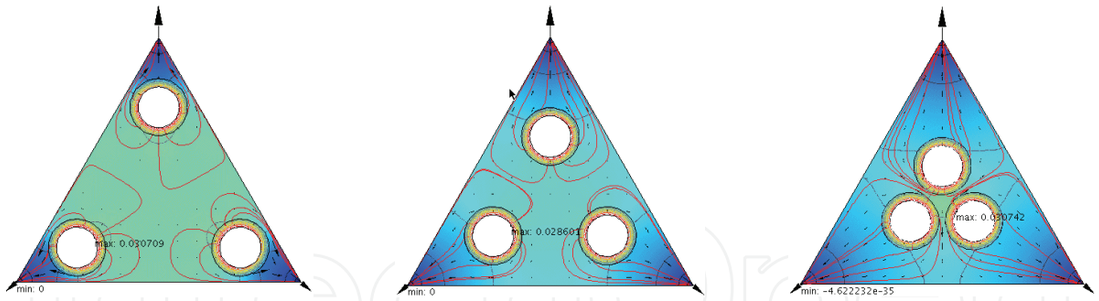

a. The wide spacing limit b. Optimal design a. The narrow spacing limit

Figure 15. The electric field in the structural optimization of the elemental system

(c) Higher order ensembles

Next, the optimal elemental system is used to build higher order ensembles. The first construct is obtained by mirroring the elemental cell with respect to its edges (Fig. 16a).

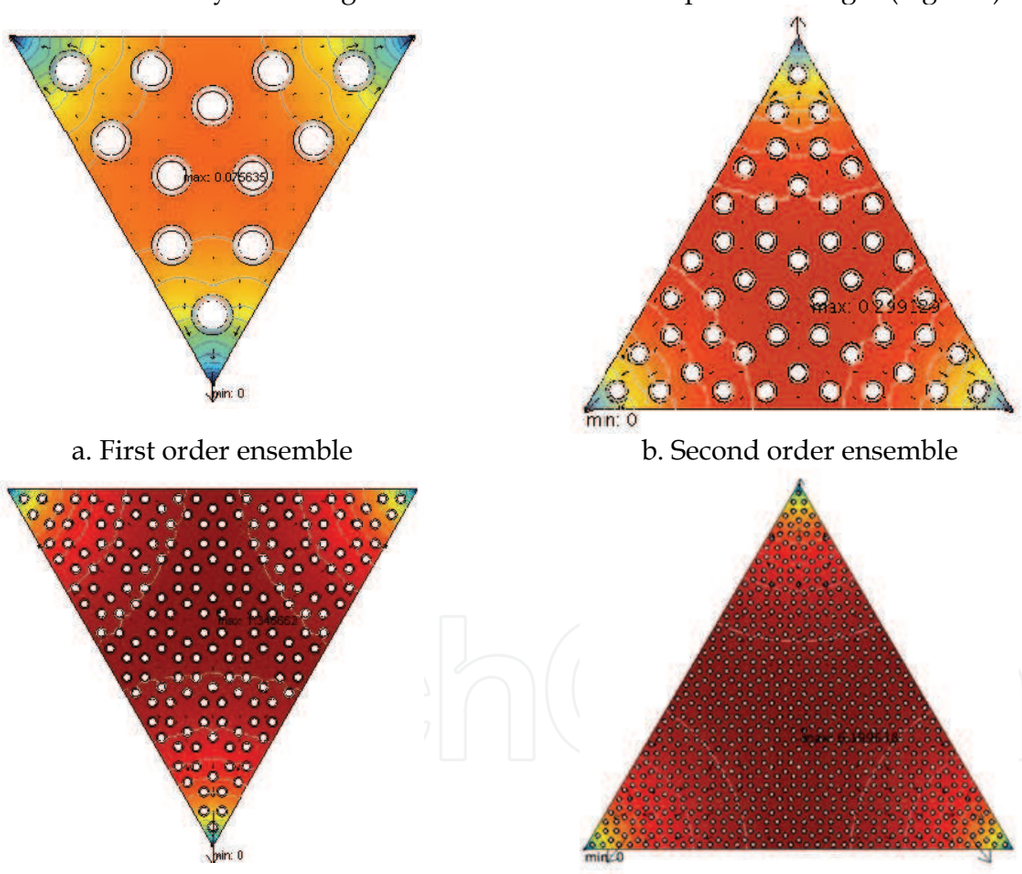

a. First order ensemble b. Second order ensemble

c. Third order ensemble d. Fourth order ensemble

Figure 16. The first four higher order SPVC ensembles – voltage and electric current

As this simple replication does not guarantee an optimum first order construct, numerical experiments (Negoias & Morega, 2005) were needed to validate the optimality of this design: *QF* was evaluated for different positions of the SPV beads along the principal lines of the first construct. There are countless layouts that might be considered, however we

used the symmetry of this design to reduce the computational domain to 1/6 of its actual size, and the SPV beads were displaced such as to preserve symmetry. The analysis confirmed the layout obtained by mirroring the elemental cell, and the reason is that the aluminum foil has a very good electrical conductivity as compared to the cells.
The mirroring technique may be pursued to generate ensembles of higher and higher order, thus propagating the triangular symmetry (Fig. 16b-d). Apparently, the inner regions are working at almost uniform voltage, and the vertices regions, acting as electrical terminals, are areas of higher voltage gradients.
Remarkably, all constructs exhibit almost the same series resistance, which is a feature of constructal structures (Morega & Bejan, 2005), (Bejan, 2000).

4.3 Honeycomb arrayed SPVC ensembles – a second model

To exemplify the influence that the elemental system has in the shape of the higher order ensembles generated by the contructal growth technique, in this subsection we report a different approach to the honeycomb SPV ensembles optimal design.
Here, we assume that by technological reasons (optimum spacing between spheres) there are no degrees of freedom in changing the size of the honeycomb (Fig. 11) – *e.g.*, (SPP, 2006). We skip the optimization sequence for the elemental system that may make the object of a distinct investigation. In this sense, our approach is *quasi*-constructal.

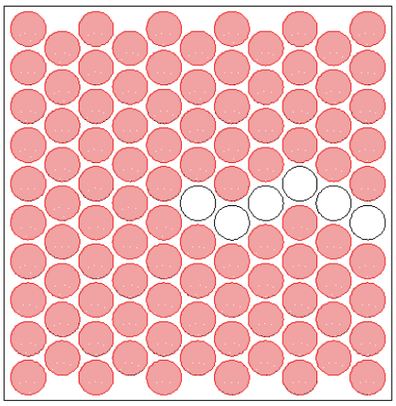

a. The elemental cell

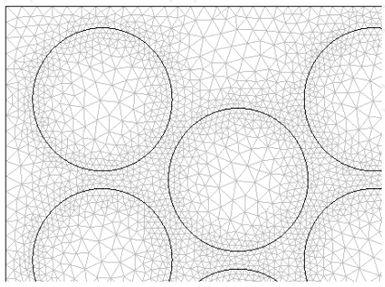

b. The FEM mesh

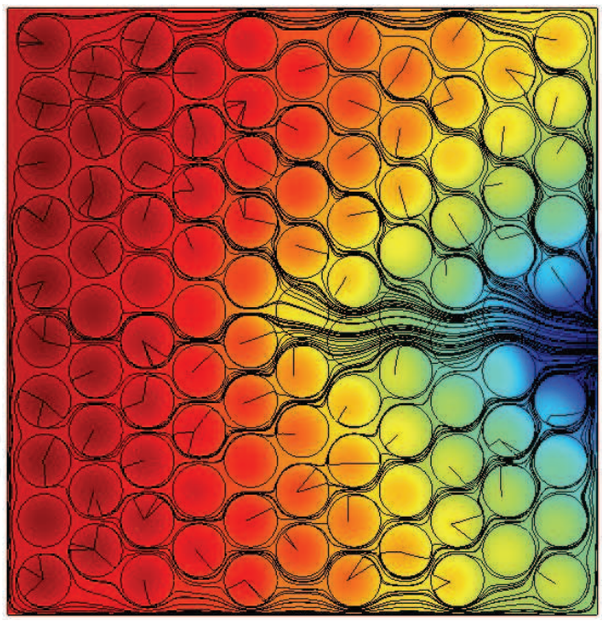

c. The electric field – the voltage distribution

Figure 17. The honeycomb SPVC elemental system

Figure 17 shows the computational domain for the elemental system for the proposed packaging. The optimization was carried out by numerical simulation, and the mathematical model is made of eqs. (10) and (11) with appropriate boundary conditions.

The coloured disks in Fig. 17a represent the SVPCs, and the white background is the aluminium cathode. The port is seen at the boundary on the right. The white disks add to the high conductivity path to the exit port. Figure 17c shows the electric field by voltage surface map and contours. The hardest working point (of the highest voltage) is farthest from the exit port (the upper and lower vertices on the left edge of the elemental cell).
Higher order ensembles are produced starting from the elemental system. Figure 18 shows the computational domains for the 1st, 2nd, 3rd, 4th order ensembles. Note that each new ensemble results by combining two, lower level optimized ensembles; in this process either one column or a row (depending on odd-even the order of the ensemble) is lost by partially overlapping the two constituent lower-level ensembles in order to preserve symmetry with an odd number of columns/rows. Also, the high conductivity path obtained by removing SPVCs preserves the same thickness in each ensemble. As seen from Fig. 18, depending on the ensemble order, the path that connects the high conductivity tree to the port on the boundary may be a either a straight or a saw-teeth-like strip.

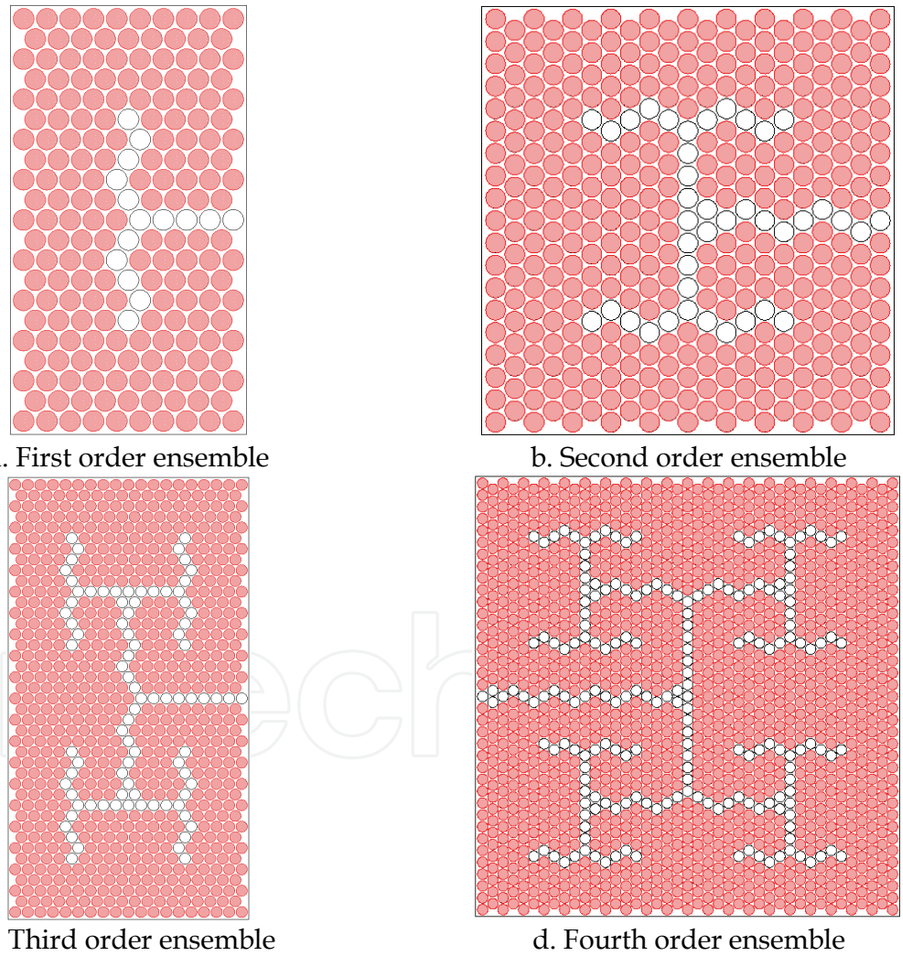

a. First order ensemble b. Second order ensemble

c. Third order ensemble d. Fourth order ensemble

Figure 18. Constructal ensembles – computational domains

Figure 19 shows the voltage distribution on the first four higher order ensembles. As the order of the ensemble increases, the tree-like structure of the highly conductive material emerges: *The tree is the flow architecture that provides the easiest (fastest, most direct) flow access*

between one point (source, or sink) and infinity of points (curve, area, or volume). Among other practical applications of tree-shaped flow architectures note the cooling of electronics (Bejan, 1997), (Ledezma et al., 1998), reconfigurable power networks (Morega & Ordonez, 2007), (Morega et al., 2006c, 2008) and the flows through porous media (Ordonez et al., 2003), (Azoumah, 2004).

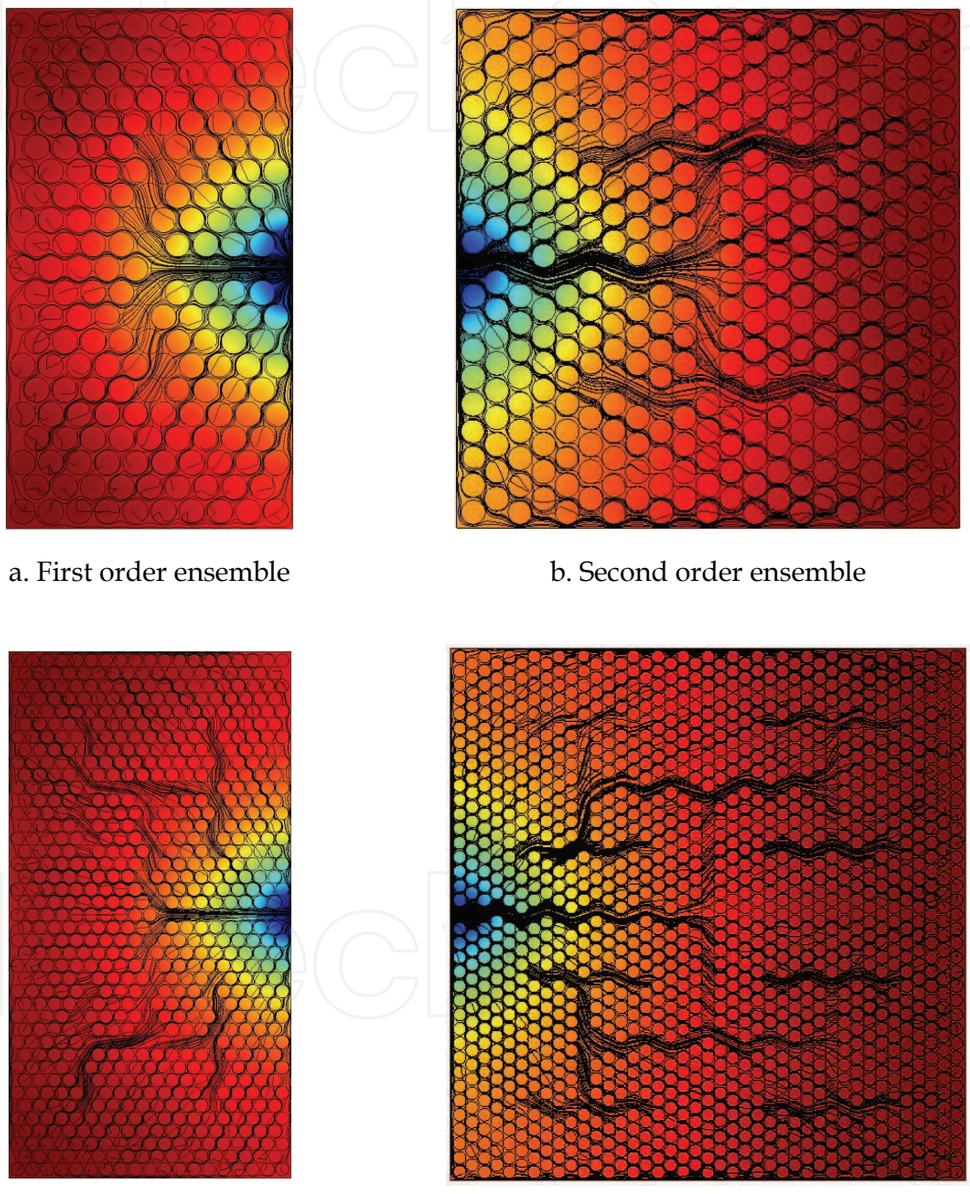

a. First order ensemble b. Second order ensemble

c. Third order ensemble d. Fourth order ensemble

Figure 19. Higher order constructal ensembles – electric field

At this point it is instructive to investigate the surface grey map in Fig. 20: the current flow in the second order ensemble. It outlines clearly the cathode foil and the high conductive tree that conveys the current to the exit port on the boundary.

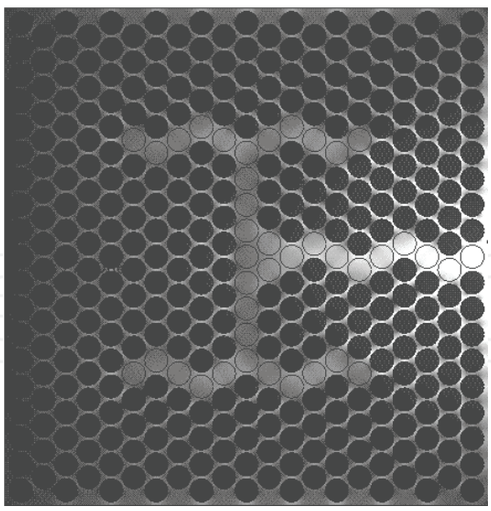

Figure 20. The cathode foil and the high conductive path evidenced by the current density spectrum in the second order ensemble

The non-dimensional maximum voltage and the series resistance obtained by numerical simulation, for different conductivities ratio, σ_p/σ_0 are given in Fig. 21a,b respectively.

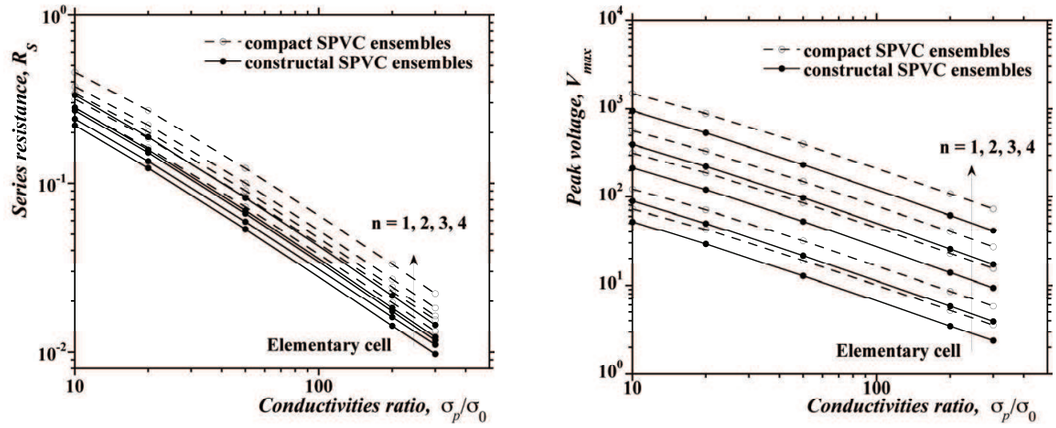

a. Maximum voltage drop b. Series resistance

Figure 21. The maximum voltage and the series resistance for the first four ensembles for the honeycomb SPV modules (non-dimensional quantities)

As expected, the higher conductivity ratio, the lower the voltage drop on the module, hence the lower the losses by series resistance. The optimized ensembles (continuous curves) have consistently lower series resistances than their unstructured counterparts (dashed curves). An important result exhibited by the optimized ensembles is that R_s does not vary with the ensemble order: this is an important feature of constructal structures and it evidences their *scalability* (Bejan, 2000). The fact that the proposed structural growth – from the elemental system to higher order ensembles – is scalable confirms – *a posterirori* – the constructal nature of the design that we adopted, imposed by the technological constrains that come with the assumed honeycomb pattern and the spherical packaging.

4.4 Wired spherical photovoltaic cells

A different technology (Kyosemy, 2006) utilizes larger-size SPV cells that are provided with two, top and bottom electrical contacts, which allow connecting the cells in ensembles through thin wires – in parallel or series – to deliver higher current and voltage. As for the honeycomb module, the spacing between cells, or the "domain of existence" for a SPVC, is not a degree of freedom in the optimization process, and it is assumed imposed by technological grounds: the spheres should not shadow each other, nor should they be too loosely packed since the module has to be compact.

The optimization process starts by assuming an elemental system made of a pair of interconnected SPVCs (Fig. 22a). As the SPVCs are embedded in an electrically insulating mass, the elemental system is reduced to a pair of the SPVCs and the interconnecting wires. All sides are insulated, except for the port where the current leaves the structure. Here too, the structural, quasi-constructal design and its optimization were carried out by numerical simulation. The mathematical model for the kinetic, DC electric field is made of eqs. (10), (11) and appropriate boundary conditions (Morega et al., 2006a).

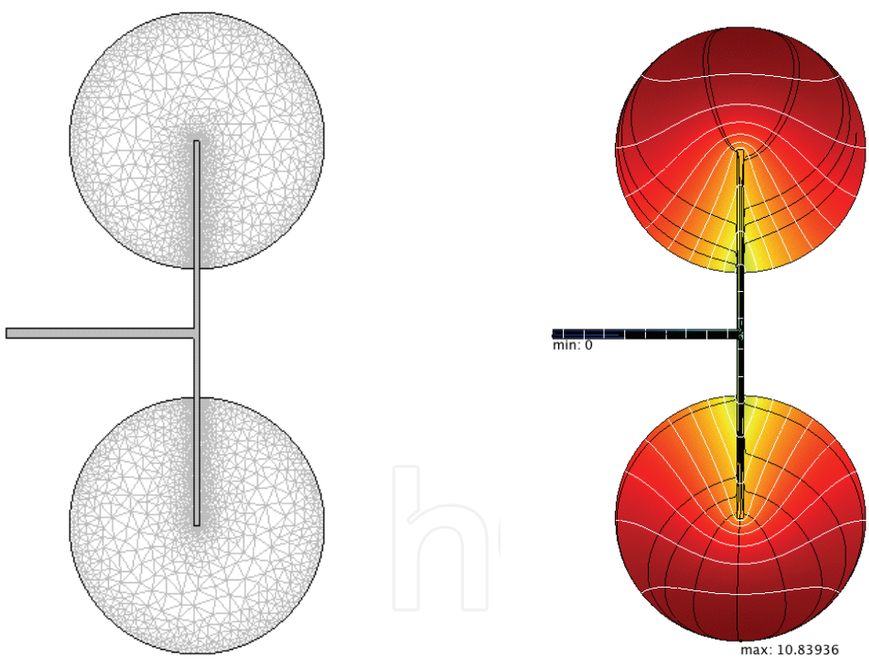

a. Computational domain b. Electric field – voltage

Figure 22. The elemental system for the wired SPVC made of pair of cells

Figure 22b shows the voltage distribution (surface color map and contour lines), and the current density path through streamlines for the elemental system.

The constructal growth follows by first merging two mirroring elemental cells. Then, two first-order ensembles are joined into a second order ensemble, and so on. Figure 23 displays the electric field through the voltage and current density spectra for the first three higher order ensembles.

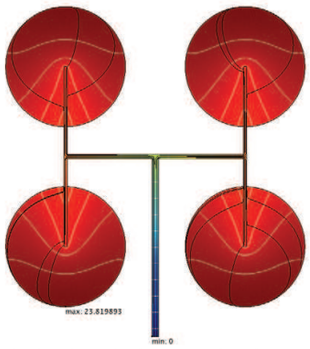

a. First order ensemble

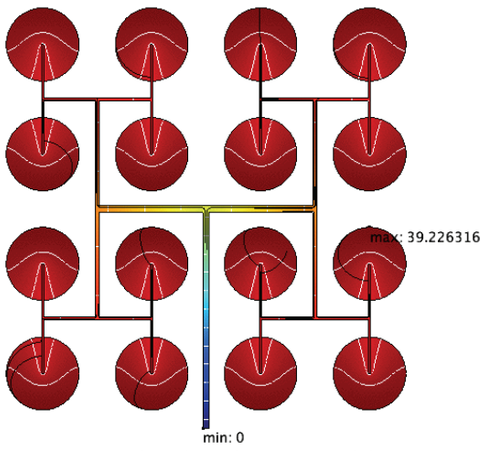

c. Third order ensemble

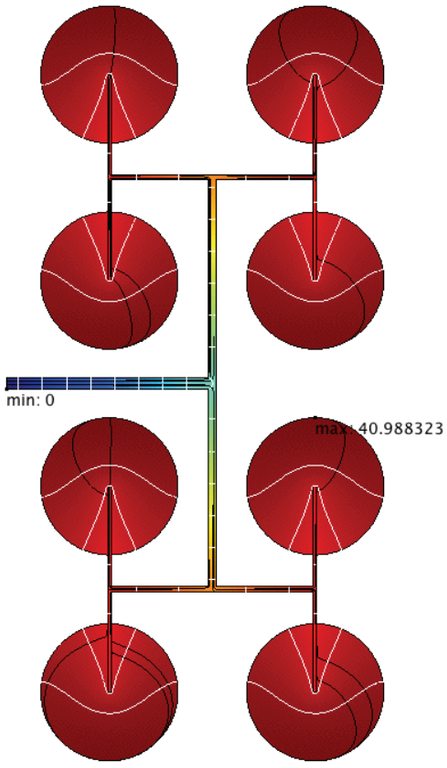

b. Second order ensemble

Figure 23. The electric field distribution for several higher order ensembles of wired SPVCs

The simulation results are synthetically presented through the maximum voltage (Fig. 24).

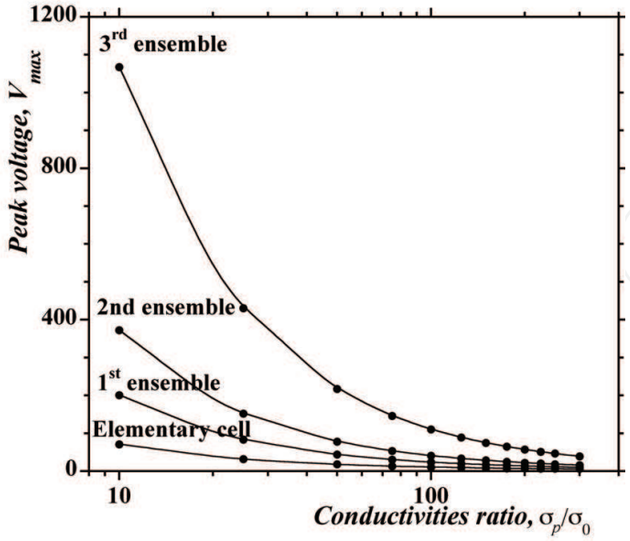

Figure 24. The maximum voltage drop for wired SPV ensmebles (non-dimensional quantities)

Apparently, V_{max} decreases as the conductivity of the high conductivity material increases.

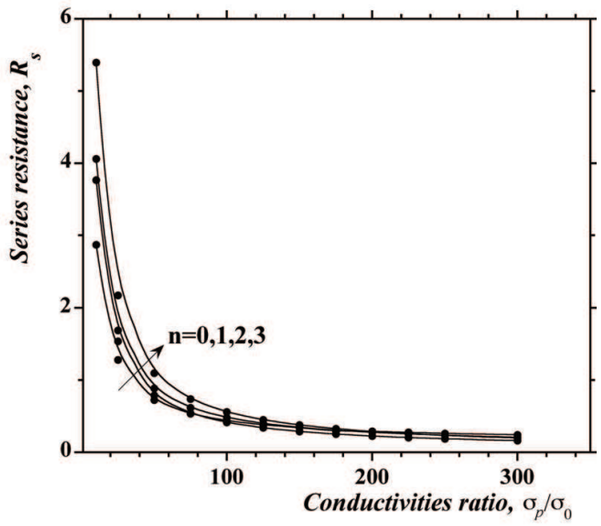

Figure 25. The series resistance for wired SPV ensembles (non-dimensional quantities)

Figure 25 shows the series resistance for the elementary cell (n = 0) and the first three higher order ensembles (n = 1, 2, 3) as functions of the conductivities ratio, σ_p/σ_0.
Clearly, the maximum voltage drops as the conductivity of the high conductivity material increases, which means that the overall voltage drop due to the series resistance is also a decaying function of σ_p/σ_0.
As for the honeycomb SPVC ensembles, these results suggest that for higher conductivities ratios all ensembles exhibit almost the same series resistance: a feature consistent with the constructal optimization process.

5. Conclusions

In the structural optimization conducted through analytic and numerical simulation the following conclusions were drawn:

- The *constructal principle* is *deterministic*, based on the outlining physical laws in the system under investigation. The optimal series resistance, R_S, of the PV ensembles are constructed starting from an elemental system, *in a time arrow from small to large*. This technique differs fundamentally from *non-deterministic* (*i.e.*, postulated) designs, *e.g.*, in a top-down sequence from higher order to lower order ensembles.
- The structural optimization used to design each building block and ensemble provides for the minimization of the PV series resistance, or optimal electrical current *access*. *The optimized ensemble exhibits the easiest access of its internal current.*
- The result of the PV R_S optimization is a structure where the total current is driven to the exterior (terminal) by the smallest voltage drop. This results also in the smallest power loss by the series resistance of the PV system.
- The starting point in the design is the optimization of the elemental system by utilizing the underlying physical laws (here, Maxwell).
- Beginning with the second order flat-surface PV ensemble, one particular rule emerges: *each new ensemble is made of two, lower order, optimized ensembles of the immediately lower level of detail*.
- Although not optimal in a strict mathematical sense, the PV ensembles of order higher than two are *the best blocks that fit together*.

- The optimization based on the analytic solution is valid when the conductivities ratio $\sigma_P/\sigma_0 >> 1$, and when the porosity $\phi_i << 1$.
- Constructal minimization of R_S leads to a design that is not only optimal: it has also a *naturally* attractive appeal, where the collector fingers are seen to evolve *naturally* into busbars. Therefore, depending on the shape of the elemental system (rectangular geometry in our analysis), the optimized structures produced by this design may cope with aesthetic criteria requested by architectural and design goals with which PV ensembles have to comply.
- Numerical simulation and the commonly available hardware resources have reached the level where they complement the design tools in engineering.

6. Acknowledgments

A.M. Morega acknowledges the "National University Research Council" for financial support trough the grant 32/358/2005-2007. J.C. Ordonez acknowledges support from the Office of Naval Research (ONR).

7. References

Altermatt, P.P.; Heiser, G.; Kiesewetter, T.; McIntosh, K.R.; Honsberg, Ch.B.; Wenham, S.R. & Green, M.A. (1977). Establishing an accurate numerical model for the 2D-simulation of buried contact cells. In *the 26th IEEE Photovoltaic Specialist Conference*, Anaheim, CA, 29 September – 3 October.

ATS – Automation Tooling Systems, Inc. (2006). Solar, Industry Note #PV1-0303.01, www.atsautomation.com

Azoumah, Y.; Mazet N. & Neveu, P. (2004). Constructal network for heat and mass transfer in a solid-gas reactive porous medium, *Int. J. Heat and Mass Transfer,* 47, pp. 2961-2970.

Bejan, A. (1997). The constructal law of structure formation in natural systems with internal flows. In: *Proc. of the ASME, Advanced Energy Systems Division, ASME*, Vol. 37, pp. 257-264.

Bejan, A. (1997). Constructal theory network of conducting paths for cooling a heat generating volume. *Int. J. Heat Mass Transf.*, Vol. 40, 4, pp. 799-816.

Bejan, A. (1993). *Heat Transfer*, New York: Wiley.

Bejan, A. (2000). *Shape and Structure, from Engineering to Nature*, United Kingdom: Cambridge U. Press, Cambridge.

Burgers, A.R. & Eikelboom, J.A. (1997). Optimizing metalization patterns for yearly yield. *26th PVSC*, Sept. 30 – Oct. 3, Anaheim, CA, USA, pp. 219-222.

Comsol, AB., COMSOL v. 3.0-3.4. (2004-2008). www.comsol.com

CPS-UNSW, Australia: Centre for Photovoltaic Engineering U. of New South Wales *Solar cells*. (2006) www.pv.unsw.edu.au

EMSOLAR – Institut für Elektrische Energietechnik, (2007). http://emsolar.ee.tu-berlin.de/~ilse/solar

Green, M. (1986). Operating Principles, Tech. & Systems Applications, In: *Solar Cells*, Australia: U. South Wales.

Horzel, J. & De Clerq, K. (1995). Advantages of a new metallization structure for the front side of solar cells. *13th EC Photovoltaic Solar Energy Conference*, Nice, France. pp. 1368-71.

Fujipream & Clean Venture, 21, (2006).
http://techon.nikkeibp.co.jp/english/NEWS_EN/20051209/111508

Viaud, M. (2004). Photovoltaic solar electricity. Part of global strategy, key lecture, *AIE Conference*, Brussels, 23 Sept.

Kyosemi - Kyoto Semiconductor Corp., (2006). www.kyosemi.co.jp/index_e.html

Ledezma, G.A.; Bejan, A. & Errera, M.R. (1997). Constructal tree networks for heat transfer. *J. Appl. Phys.* 82, pp. 89–100.

Lemmons, D.S., (1997). *Perfect form*, Princeton Univ. Press, Princeton, NJ.

Morega, A.M., (1998). *Numerical modeling of boundary value problems in engineering* (in Romanian, MatrixRom, ISBN 973-9390-05-6.

Morega, A.M. & Bejan, A., (2005). A Constructal Approach to the Optimal Design of Photovoltaic Cells, *Int. Journal of Green Energy*, **2**, 3, pp. 233-242.

Morega, A.M.; Ordonez, J.C.; Negoias, A.P. & Hovsapian R. (2006). Spherical photovoltaic cells – A constructal approach to their optimization, *OPTIM 2006*, May 22-24, Brasov, Romania.

Morega, A.M.; Ordonez, J.C.; Negoias, P.A.; Morega, M. & Hovsapian, R. (2006). Optimal electrical design of spherical photovoltaic cells, *COMSOL Conference*, Congress Center of the Czech Technical University, Prague, October 26.

Morega, A.M. & Ordonez, J.C. (2006). Constructal Design of Concurrent Power Distribution Networks, *COMSOL Conference*, Boston, October 20-21, Hyatt Regency, Cambridge, Boston, MA, USA.

Morega, A.M.; Ordonez, J.C. & Morega, M. (2008). A constructal approach to power distribution networks design, *International Conference on Renewable Energy and Power Quality*, ICREPQ'80, 12-14 March, Santander, Spain.

Negoias, A.P., Morega, A.M., (2005). Constructal Optimization of Spheral Photovoltaic Cells, *Mathematical Modeling of Environmental and Life Sciences Problems*, *3rd Workshop*, 7-10 September, Constanta, Romania.

Ordonez, J.C.; Bejan, A. & Cherry, R.S. (2003). Designed Porous Media: Optimally Nonuniform Flow Structures Connecting One Point With One or More Points. *International Journal of Thermal Sciences*, Vol. 42, pp. 857-870.

Poincaré, H. (1902). *Science and hypothesis* (in English), London and Newcastle-on-Cyne (1905): The Walter Scott publishing Co.

Radike, M.; Summhammer, J.; Breymesser, A. & Schlosser, V., (2002). Optimization of artistic contact patterns on multicrystalline silicon solar cells, *2nd Photovoltaic Solar Energy Conference*. Vienna, Austria www.ati.ac.at/~summweb.

Travers, D.; Watt, M.; MacGill, I.; Kaye, J.; Kunzi, S. & Spooner, T. (2001). Evaluation tool for building integrated photovoltaic systems. Australia: Photovoltaics Special Research Center, School of Electrical Engineering, Univ. of New South Wales, Sydney, NSW.

Treble, F.C. *Ed*. (1991). *Generating electricity from the sun*. (Ifac Symposia Series), Pergamon Press, ISBN13 9780080409368, Oxford, UK.

SSP – Spheral Solar Power (2006), www.sspsolar.com

Verbeek, M. & Metz, A. (1996). Mechanically grooved high-efficiency Si solar cells with self-aligned metallization. *25th IEEE Photovoltaic Specialists Conference*, Washington DC, USA, pp. 521-524.

STARFIRE, *Photovoltaics Technical Information Guide*, Sc. Ed., Solar energy research institute, http://starfire.ne.uiuc.edu/ne201/course/topics/solar_thermal/

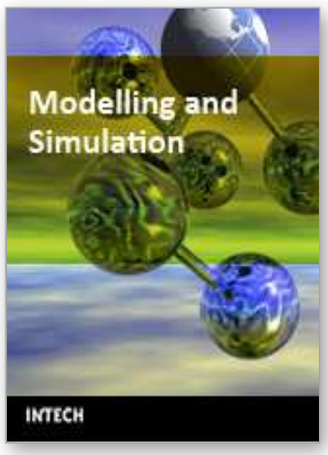

Modelling and Simulation

Edited by Giuseppe Petrone and Giuliano Cammarata

ISBN 978-3-902613-25-7
Hard cover, 688 pages
Publisher I-Tech Education and Publishing
Published online 01, June, 2008
Published in print edition June, 2008

This book collects original and innovative research studies concerning modeling and simulation of physical systems in a very wide range of applications, encompassing micro-electro-mechanical systems, measurement instrumentations, catalytic reactors, biomechanical applications, biological and chemical sensors, magnetosensitive materials, silicon photonic devices, electronic devices, optical fibers, electro-microfluidic systems, composite materials, fuel cells, indoor air-conditioning systems, active magnetic levitation systems and more. Some of the most recent numerical techniques, as well as some of the software among the most accurate and sophisticated in treating complex systems, are applied in order to exhaustively contribute in knowledge advances.

How to reference

In order to correctly reference this scholarly work, feel free to copy and paste the following:

Alexandru M. Morega and Juan C. Ordonez (2008). Multiphysics Modelling and Simulation in Engineering, Modelling and Simulation, Giuseppe Petrone and Giuliano Cammarata (Ed.), ISBN: 978-3-902613-25-7, InTech, Available from: http://www.intechopen.com/books/modelling_and_simulation/multiphysics_modelling_and_simulation_in_engineering

INTECH
open science | open minds

InTech Europe
University Campus STeP Ri
Slavka Krautzeka 83/A
51000 Rijeka, Croatia
Phone: +385 (51) 770 447
Fax: +385 (51) 686 166
www.intechopen.com

InTech China
Unit 405, Office Block, Hotel Equatorial Shanghai
No.65, Yan An Road (West), Shanghai, 200040, China
中国上海市延安西路65号上海国际贵都大饭店办公楼405单元
Phone: +86-21-62489820
Fax: +86-21-62489821

IntechOpen